



Article

Forecasting the Urban Expansion Effects on the Design Storm Hydrograph and Sediment Yield Using Artificial Neural Networks

Dimitrios Myronidis ^{1,*}  and Konstantinos Ioannou ² 

¹ School of Forestry and Natural Environment, Aristotle University of Thessaloniki, 54124 Thessaloniki, Greece

² Forest Research Institute, Hellenic Agricultural Organization ‘Demeter’, Vasilika, 57006 Thessaloniki, Greece; ioanko@fri.gr

* Correspondence: myronid@gmail.com; Tel.: +30-2310-992736

Received: 25 October 2018; Accepted: 18 December 2018; Published: 24 December 2018



Abstract: Urban expansion substantially alters the impervious areas in a catchment, which in turn affects surface runoff and sediment yield in the downstream areas. In this study, the Land Transformation Model (LTM) was used to forecast the urban land expansion in a catchment, whilst future land use maps were employed according to the Soil Conservation Service Curve Number method (SCS-CN) and the Modified Universal Soil Loss Equation (MUSLE) model, so as to examine the urbanization effects on runoff and sediment yield production respectively. Compared to pristine conditions, urban land is anticipated to increase from 6% in 1979 to 31% by 2027. The latter expansion pointed to an increase of peak discharge by 2.2–2.6 times and of flood volume by 1.6–2.1 times, with the sediment yield ranging between 0.47 to 1.05 t/ha for the upcoming 2027 period. Furthermore, the urban sprawl effects on all the latter variables were more profound during short duration storm events. Forecasting urban expansion through integrated artificial neural networks (ANN) and geographic information system (GIS) techniques, in order to calculate the associated design storm hydrograph and sediment yield, is of great importance, in order to properly plan and design hydraulic works that can sustain future urban development.

Keywords: LTM; urban expansion; ANN; SCS-CN; MUSLE

1. Introduction

Since 1950, the global urban population has rapidly increased from 751 million to 4.2 billion in 2018 and by 2050 two thirds of the world’s population is expected to live in urban areas [1]. The same pattern is evident in Europe too, since almost three quarters of the European population lived in an urban area in 2015, whereas no more than half of the European population was living in an urban area in 1950 [2]. Moreover, the urban population in the US has grown by nearly 500% since 1910, while the rural population has grown by only 19%; in 2010, 81% of the U.S. population was considered to be urban [3]. In Greece, which has suffered greatly due to eight hard years of economic recession and although employment rates are higher in rural rather than urban areas, nevertheless 79.1% of its population is still living in urban areas [1,2].

This global rapid urban population growth trend is associated with an accelerated urban sprawl, which may offer certain important benefits to the urban population in terms of higher employment rates, better infrastructure and a higher income but is also associated with some adverse effects on the environment and on natural resources. Due to the urban sprawl, the mean annual surface air temperature in cities has been undergoing excessive warming [4], the habitat potential and biodiversity

have been negatively impacted by the degree of urbanization [5] and the hydrologic cycle and in stream process have been altered [6]. These changes could seriously impact the mountain rivers sediment production and transport [7] with significant changes in the bed morphology [8] and floods with a high content of transported sediments and debris floods can occur [9]. Moreover, the temporal and spatial scales of these phenomena may vary greatly during intense precipitation events with respect to normal conditions [10].

In recent decades, a water budget or hydrologic model have been commonly utilized [11,12] to evaluate the effects of the recorded urban expansion on the hydrology of catchments, so as to model the effects of different land use change scenarios on runoff and sediment yield [13,14]. However, since land use planners and policy makers are more and more interested in predicting urban expansion and its effect on natural resources, much of the research in recent years has focused on the coupling of hydrologic models with sophisticated spatial land use change (LUC) models, that are able to project LUC changes in the near future. LUC models can be used as tools for studying the human effect on the Earth's surface and to forecast land change into the future [15].

LUC models use a variety of techniques, including linear extrapolation, suitability mapping, genetic algorithms, neural networks, scenario analysis, expert opinions, public participation and agent-based modelling, in order to produce a prediction map for the near future [16]. However, there are three main stream approaches for LUC models: models which rely primarily on economic models and data [17–19], models that rely equally on multiple approaches and data to determine cause and effect relationships [20–22] and models that are role-based analyses, where a norm is established to allocate LUC-related impacts [23–26].

The objectives of the present paper are: firstly, to use three reference land use maps of the Elaionas catchment for the years 1979, 1996 and 2007 in the Land Transformation Model (LTM) [27,28], so as to forecast the urban sprawl for the year 2027; secondly, based on both the recorded land use changes and the future urban sprawl scenarios developed by the LTM, to examine the effects of current and future urban expansion on the design hydrograph, and, thirdly, to estimate the impact of urban sprawl on the associated sediment yield generated by the latter storm events.

The Land Transformation Model (LTM) used for forecasting future LUC was created by the Human-Environment Modelling and Analysis Laboratory of Purdue University [28] and is based on the coupling of an Artificial Neural Network (ANN) with a Geographic Information System (GIS), in which the latter was used to provide the inputs for the ANN. Although there are many machine learning models such as extreme learning machine, support vector machine, adaptive neuro-fuzzy inference system and deep learning models the ANN was selected in this study because the LTM predefined tool box is broadly used worldwide so as to forecast land use evolution [29]. These inputs are used to train and test the neural network in order to generate a numerical solution between the input and the output, expressed as a future urban area prediction map for the year 2027. The hydrologic response of the catchment to urban sprawl, in terms of observed changes in the design storm hydrograph, is modelled through the usage of the popular Soil Conservation Service (SCS) Synthetic Unit Hydrograph (SUH) method [30], whereas the synthetic unit hydrographs were provided by applying the SUH theoretical framework methods and not from the utilization of any commercial software, such as the Hydrologic Modelling System (HEC-HMS) [31] or the Catchment Modelling System (WMS) [32]. Finally, the Modified Universal Soil Loss Equation (MUSLE) model [33] was chosen so as to calculate the associated sediment yield volume that was produced due to the aforementioned design storm events. The efficiency of the MUSLE model in estimating design storm related sediment yield has been proven by several international studies, through the comparison of sediment yield values that were measured and predicted using the MUSLE model [34–36]. Although that the MUSLE model has provided good results in many areas throughout the world, limitations of such equation are that local deposition is not explicitly taken into account, as well as that it has been applied here in a context that is different from that for which it has been developed [37].

This approach of coupling a dynamic land use change (LUC) model with a hydrologic model has been used by various other researchers in an effort to make estimations regarding the effect of future land usage scenarios on the hydrologic cycle. Tang et al., (2005) use the LTM model to predict future land use changes in the U.S. Muskegon catchment and to forecast and assess the impact of the predicted land use changes on long-term runoff [38]; Wayland et al., (2002) modelled the impact of historical and predicted land use change on surface water quality using ground water flow and solute-transport models [39]; Lin et al., (2007) employed the simulated land use scenarios derived from the application of the conversion of land use and its effects (CLUE-s) LUC model in a lumped hydrological model, so as to reveal the differences to the annual streamflow and groundwater discharge due to urbanization [40]. Furthermore, the effects of urbanization on annual runoff and flood events were also assessed through the pairing of the Wayland software, which was used to calculate runoff generation and the integrated Markov Chain and Cellular Automata model, which was used to develop future land use maps [41]. However, to the authors' knowledge, a study that predicts the impact of future urban expansion on the design storm hydrograph and the associated sediment yield magnitude has never been published before.

2. Study Area, Datasets and Past Urban Sprawl Description

The catchment under study is situated in Northern Greece, uphill from the city of Thessaloniki, which is the second largest city in Greece, with a population of 789,191 inhabitants, according to the 2011 census [42]. It encompasses almost half the area of the surrounding urban forest, as is illustrated in the following orthorectified aerial imagery of 1996 (Figure 1) [12]. The 1:50,000 scale topographic maps of the study area obtained from the Hellenic Military Geographical Service (HMGS) were used to create a digital geodatabase, containing the catchment boundary, the drainage network and the 20-m interval contour map layers, all projected at the GGRS1987 geographic coordinate system and to generate a digital elevation model (DEM) at a 10-m spatial resolution, which is considered sufficient for most DEM-based geomorphic and hydrologic modelling applications [43]. The catchment drainage area is approximately 18.62 km² and the altitude ranges from 60 to 560 m. A fourth-order dendritic pattern ephemeral stream, based on [44] ordering system, with a total length and main stream slope, equal to 8.365 m and 5.8% respectively, extends across the catchment and traverses the ring road and the city, before spilling into the Thermaikos Gulf.

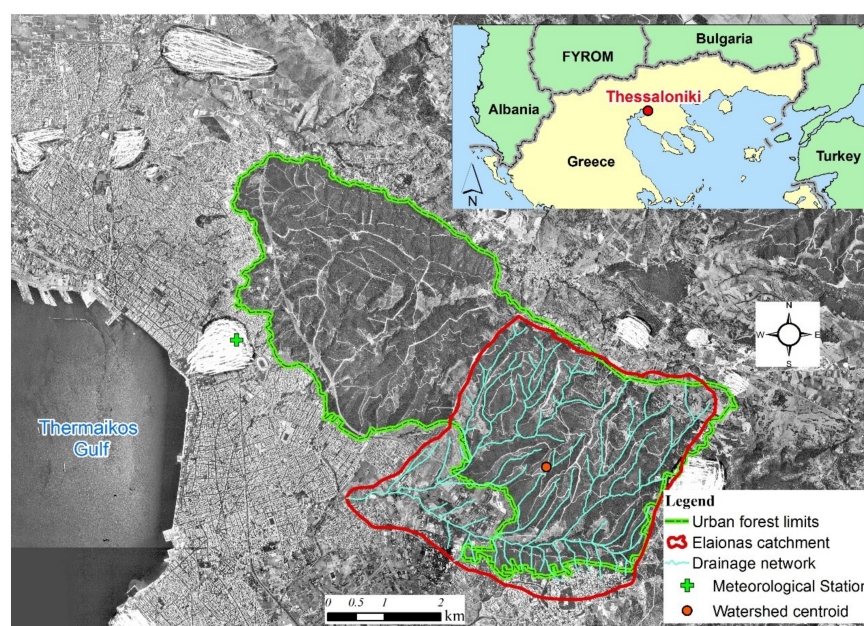


Figure 1. Location map and spatial location of the rainfall gauge (images courtesy of National Cadastre and Mapping Agency S.A.).

The weather station of the Department of Meteorology and Climatology of the Aristotle University of Thessaloniki is located within the University Campus, just 6 km away from the catchment centroid (Figure 1) which was designated with typical GIS techniques and provided the hourly rainfall dataset covering the period 1947–2003 [45]. The city has a typical Mediterranean climate, characterized as Hot-summer Mediterranean climate Csa according to the [46] classification, with a rainy winter season from October to March and hot dry summers. The mean annual precipitation is 451.7 mm and its standard variation is ± 96.3 mm, whilst the precipitation variation is binomial, with the principal maximum and minimum observed in December and August respectively [47].

The 1:50,000 scale geological map of the National Institute of Geology and Mineral Exploration (IGME) revealed that the catchment's bedrock is composed of quartzitic sandstone (18%) and limestone (3.9%), which outcrop the headwaters, gneiss (28.1%) in the middle part and red silty clays (50.0%) that encompass the downstream part of the catchment. Furthermore, the soil texture characteristics, based on the U.S. Department of Agriculture (USDA) classification scheme, which were derived from the combined clay, silt and sand maps, were obtained from the European Soil Data Centre [48]. The latter dataset revealed that the catchment texture is dominated by Loam soils (50.8%), whereas sandy loam, sandy clay-loam and clay-loam soils encompass 26.4%, 20.1% and 2.7% of the catchment respectively.

The study area has experienced decades of intensive land use changes in the past, such as urbanization, deforestation and wildfires, which have highlighted the accelerated rates of urban sprawl, which are associated with the significant and rapid socio-economic growth noted in the area. The diachronically formulated artificial stream-channel modifications and registered urban expansion typically lead to a significant increase in flood hazard downstream [49]. Land use and land cover patterns for four periods between 1968 to 2007 were mapped using aerial photographs, vertical frame photographs and a Google image in ERDAS Imagine Essentials 9.3 from Leica Geosystems spatial analyst software [12] and it was revealed that, between 1968 and 2007, the urban area has increased more than fivefold, from 3.71% to 19.03% of the study area. Currently, the study area is under significant constant pressure, so as to expand the urban plan and establish new large building projects.

3. Materials and Methods

3.1. Future Urban Expansion Prediction Using Artificial Neural Networks and LTM

Artificial Neural Networks (ANNs) are computing systems inspired by biological neural networks, which are part of every living organism. ANNs are used for prediction, pattern recognition and clustering. A neural network consists of a number of elements called neurons. Each neuron receives a number of signals which are called inputs. Each neuron is internally defined by certain states which determine whether the received signal will be transmitted to another neuron or not (threshold value). In addition, when the signal is transmitted, it is coupled with an internal weight coefficient, which essentially determines how closely the specified neuron is to the receiving one. This value fluctuates at a specific interval, for example, the interval between 1 and 0, although this interval is an arbitrary choice and depends on the problem we aim to solve. The meaning of the weight value is to show us how important the contribution of the specified signal is to the configuration of the network structure for the two neurons that it connects. Each neuron has only one output, which is a function of the input signals [50–53]. The ANN in this project is a feed forward network with one input layer, one hidden layer and one output layer. The Simple Backpropagation Algorithm was used as the learning process. SNNS (Stuttgart's Neural Network Simulator version 4.2 developed at University of Stuttgart, Stuttgart, Germany) was used for the design, training and prediction of the ANN. After experimenting with a variety of architectures, we determined that the optimum number of hidden nodes is 10. Finally, the logistic function was used as an activation function.

In order for the network to be sufficiently trained, some input data must be used. This means that we must supply the network with some prototypes as inputs (in our case, maps for the years 1979 and

1996) for which we know what the output should be (a map for the year 2007). The maps from 1979 and 1996 were used for training the ANN for the year 2007. The train result for the year 2007 was compared with the actual map of that year and the prediction accuracy was determined. The trained ANN predicted land uses for the year 2027 because it was considered that there should be a significant leap in the future in order to determine urban expansion effects.

The back propagation algorithm was used to perform the training. This algorithm transfers the errors produced in the outputs during the training period backwards to the neurons used to produce the output. The errors are used to change the weights used to produce the output and thus improve the produced outputs.

For the application of the algorithm, we used two values as inputs (the distance from the road network and the distance from the stream network) and one value as output (the areas with urban land uses). These distances are calculated by implementing the Euclidian distance tool which is incorporated in ArcGIS. This tool calculated the distance of each cell to the closest source, in our case the road and stream network. The areas with urban land uses are considered as outputs and are used as the results of the ANN. The datasets of the input values were converted to 1 and all other data were set to 0, using the reclassify tool of ArcGIS, thus allowing the ANN to recognize the input data (the driver) to be used for the purpose of training [54].

To avoid over-training of the network [55], the neural network was trained with a partial set of data by providing it with data from every other cell in the county. To further reduce over-fitting, the cells in a cycle were first presented to the network in random order [56]. A cycle is defined as one complete presentation of all training cells to the network. The network was trained with the training data and the overall mean squared error generated by SNNS and each cycle was stored in a file for analysis. Based on these results, it was concluded that about 25,000 cycles were adequate to stabilize the error level to a minimum value. Thus, each model run was set for 25,000 cycles, which meant that the entire pattern file would be presented to the network 25,000 times. At the end of training, the neural network can be further tested on an additional independent validation set [51,52,57].

The Land Transformation Model used in order to predict LUC is based on the implementation of five distinct steps. The first step includes the determination of the parameters and the initial creation of the ANN as well as the network file. The second step includes all the necessary modifications in order for the maps to be expressed as text files (of 0 and 1) in order to be used by the network. These text files are then used as inputs to the ANN and also for the creation of pattern files. The next step incorporates these pattern files in the network in order to be used for training the ANN. This is done by a special batch file which is named batchman. The results are then stored in a result file (res file). The fourth step is then initiated in order for the trained network to be used against real data which were a part of the initial maps. The results are then converted into maps using a specially written batch file which converts them into ArcGIS shape file and are compared with the actual maps; more details on this method can be found in References [58,59]. Moreover, the Kappa coefficient is also calculated.

It is very crucial for the correct application of the methodology to accurately determine the drivers that affect land use change. In our case, the affecting drivers were: the transportation network and the proximity to streams. Following the determination of the drivers, we digitized the area of interest and created the subsequent raster files for the years 1979 and 1996. Therefore, the map from the year 1979 was selected to act as a baseline and the monitored urban expansion was based on that year.

3.2. Hydrologic and Sediment Yield Modelling

The effective hydrological design of water control structures that ensures both the structure safety and downstream development largely depends on the selection of the precise design discharge value that will be routed through the water system. Past experience shows that, according to the planned structure type, for example, a culvert, a flood hazard map or a dam, it is necessary to compute the design inflows to the water system generated by 20 [60], 50 [61] and 100 [62] year return period flood events respectively, so as to achieve the optimal hydraulic structure design [63]. Moreover, catchment

sediment yield estimates can be used to prioritize the checked dam construction [64], as to the most effective ways to conserve soil and water, slow down erosion [65] and control sediment transport to downstream areas [66]. However, since most catchments worldwide are ungauged and there are usually no long-term streamflow records available, the desired design discharges can be generated through the use of Synthetic Unit Hydrograph (SUH) methods [31,32].

This article focuses on design flood events with 50 and 100-year return periods and durations of 6, 12 and 24 h, which are typically associated with the design of urban drainage, flood hazard maps and dams. The design precipitation hyetograph can be developed using an Intensify-Duration-Frequency (IDF) curve, which is readily available for the study area and is obtained by fitting the Extreme Value Type I (EVI) theoretical distribution [67] to the annual extreme rainfalls of different durations for the weather station of the Department of Meteorology and Climatology at the Aristotle University of Thessaloniki [45], as is shown below:

$$i = \frac{19.77 \cdot T^{0.1909}}{t^{0.79}} \quad (1)$$

where i is the rainfall intensity (mm/h), T the return period (years) and t the rainfall duration (h).

By employing Equation (1), six rainfall intensities were computed for the design rain events with 81 and 140-year return periods, that correspond to design flood return period events of 50 and 100 years [68] and for rain durations of 6, 12 and 24 h. Each storm event precipitation depth (mm) was then calculated, as the product of its rainfall intensity with its duration. Once the total rainfall amount was specified, the storm hyetograph was generated by applying the Alternative Block Method (ABM); more details on this method can be found in Reference [63].

The amount of precipitation (mm) that is transformed to runoff (effective precipitation) can be found according to the Soil Conservation Service Curve Number method [69], as follows:

$$P_e = \frac{(P - 0.2 \cdot S)^2}{P + 0.8 \cdot S} \quad (2)$$

where P_e is the effective precipitation, P the total precipitation and S the maximum potential for soil retention. Equation (2) shows that if the rain event is less than 20% of the S , then the effective precipitation is equal to 0. Moreover, the surface storage (mm) of soil (S) is computed by:

$$S = \frac{25,400}{CN} - 254 \quad (3)$$

where CN (Curve Number) is the dimensionless index developed by the USDA Natural Resources Conservation Service [30] that ranges from 0 (maximum infiltration) to 100 (zero infiltration), whilst its value depends on land use, soil type and the Antecedent Moisture Conditions (AMC). The transformation of the effective precipitation into a runoff hydrograph is realized through the usage of the SCS unit hydrograph method [70], by computing the storm hydrograph from a 1 mm rainfall event as follows:

$$Q_p = \frac{0.208 \cdot A}{t_p} \quad (4)$$

$$t_p = t_L + \frac{D}{2} \quad (5)$$

where Q_p and t_p are the peak flow (m³/s) and the time to the peak (h) of the unit hydrograph respectively, A the catchment area (km²), t_L the lag time between the centre of mass of excess rainfall and the peak of the unit hydrograph (h) and D the duration of the effective rainfall. The lag time in hours can be computed by [71]:

$$t_L = \frac{L^{0.8} \cdot (2540 - 22.86 \cdot CN)^{0.7}}{14,104 \cdot CN^{0.7} \cdot Y^{0.5}} \quad (6)$$

where L is the hydraulic length (m), CN the runoff curve number and Y the average catchment slope (m/m). Once the peak discharge and the time of peak were calculated, the unit hydrograph was derived from the SCS dimensionless hydrograph [30]. The final flood hydrographs were computed based on the unit hydrograph and the effective rainfall hyetograph by employing the discrete convolution method; more details on this method can be found in References [63,72,73].

The estimation of the associated sediment yield, which is produced by the six rainfall events for the different land use conditions, was derived through the use of the MUSLE equation [33], as follows:

$$S = 11.8 \cdot (Q \cdot q_p)^{0.56} \cdot K \cdot L \cdot S \cdot C \cdot P \quad (7)$$

where S is the sediment yield from an individual storm (tones), Q the storm runoff volume (m^3), q_p the peak runoff (m^3/s) and K , L , S , C and P , the soil erodibility ($Mg MJ^{-1} mm^{-1}$), slope length (dimensionless), slope steepness, crop management and soil erosion control practice respectively, factors similar to the Universal Soil Loss Equation (USLE) model [74]. The L and S factors reflect the topography effect on soil erosion and together they constitute the topographic factor (LS).

4. Results

4.1. Future Urban Expansion Prediction

After the determination of the drivers affecting urbanization, we created two maps using the Euclidean distance tool. The stream distance map and the road distance map are presented in the Figure 2.

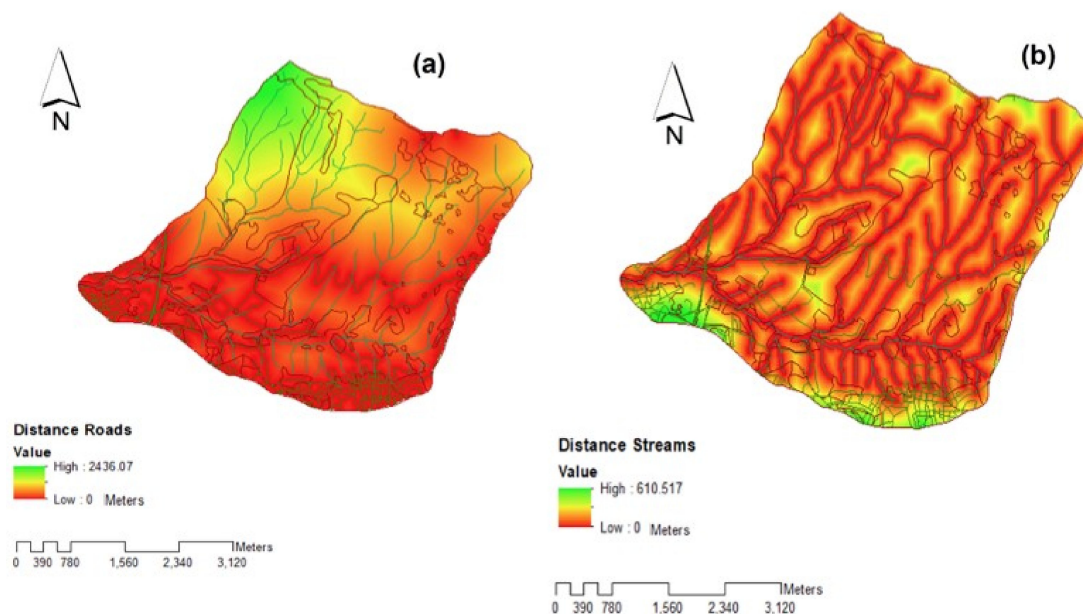


Figure 2. Euclidean distances from the Road Network (a) and Stream Network (b).

Areas depicted in red are closer to the existing stream network and areas in yellow and green are farther from it. Similarly, as regards the distance from the road network map, areas in red are closer to the road network, whereas areas in yellow and green are farther away. Using the 1979 map as a baseline, we performed a reclassification of the land uses focusing on urban uses (Figure 3).

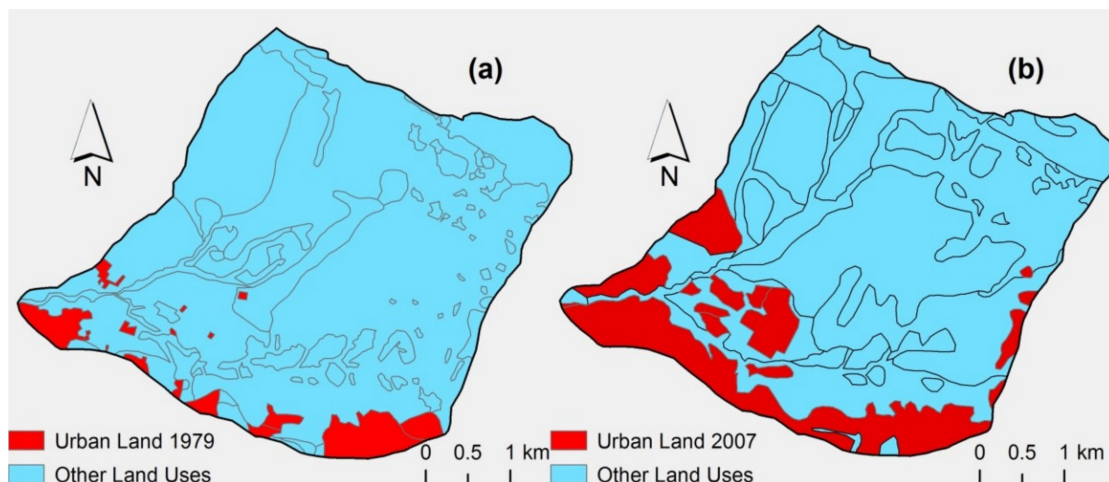


Figure 3. Land uses for the years 1979 (a) and 2007 (b).

The same process was also followed for the year 2007. These two maps were then used to train the ANN, the first as input to the network and the second as an output using the back propagation algorithm. The ANN training produced adequate results after 50,000 training cycles; it is evident in Figure 4 that no significant improvement of the Mean Square Error (MSE) is to be expected after the last cycle completion.

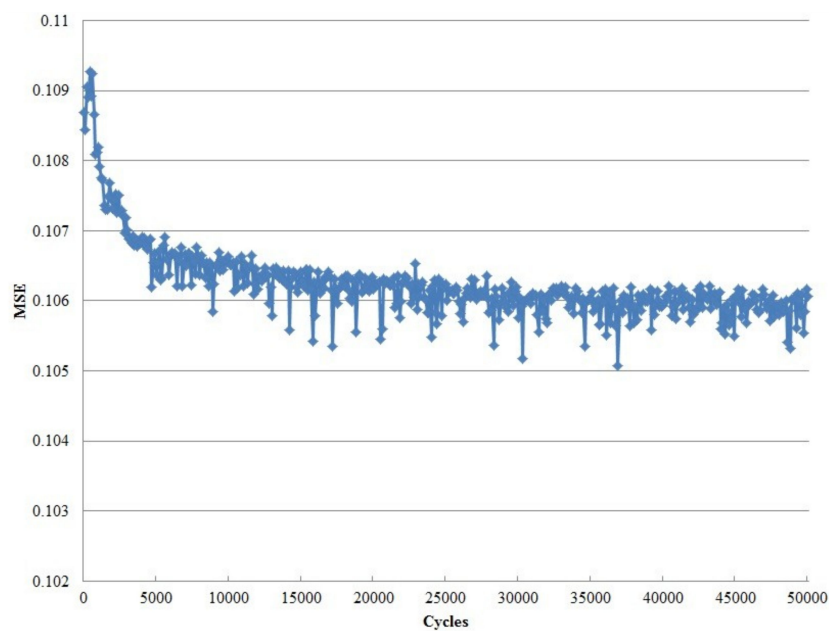


Figure 4. MSE error after model training.

The quality of the end results and thus the quality of the prediction were estimated using the Cohen's Kappa (Kappa coefficient). This measure of quality estimation is used when binary variables are used to measure the same thing. Kappa measures the percentage of data values in the main diagonal of the table and then adjusts these values for the amount of agreement that could be expected due to chance alone [28]. The equation for the Kappa coefficient is:

$$K = \frac{P(A) - P(E)}{1 - P(E)} = \frac{\sum_{i=1}^c p_{ii} - \sum_{i=1}^c p_{iT} \cdot p_{Ti}}{1 - \sum_{i=1}^c p_{iT} \cdot p_{Ti}} \quad (8)$$

where,

$i = 1, \dots, c$: the common categories of change in both observed change and simulated model run results. There are two categories (i.e., $c = 2$) categories whose values are predefined '0' (no urban change) and '1' (urban change).

p_{iT} : the proportion of cells in category i of observed change, taken from the marginal totals of the last column of the contingency matrix.

p_{Ti} : the proportion of cells in category i of simulated model run, taken from the marginal totals of the last row of the contingency matrix.

p_{ii} : the proportion of cells in the same category, i , on both observed changes and simulated model runs, taken from the diagonal elements of the contingency matrix.

$P(A) = \sum_{i=1}^c p_{ii}$: the fraction of agreement or sensitivity coefficient.

$P(E) = \sum_{i=1}^c p_{iT} \cdot p_{Ti}$: the expected fraction of agreement subject to the observed distribution.

The trained ANN produced a Kappa coefficient of 0.15. The coefficient is rather low, mainly due to the fact that we did not have enough information about the study area in the form of area maps. The result would significantly improve, if we used more datasets (i.e., more years) in order to perform our prediction. Finally, after the completion of the training session, we used the model to perform a prediction of land use change (and the appearance of urbanization) for the year 2027 (Figure 5) using maps for the year 2007.

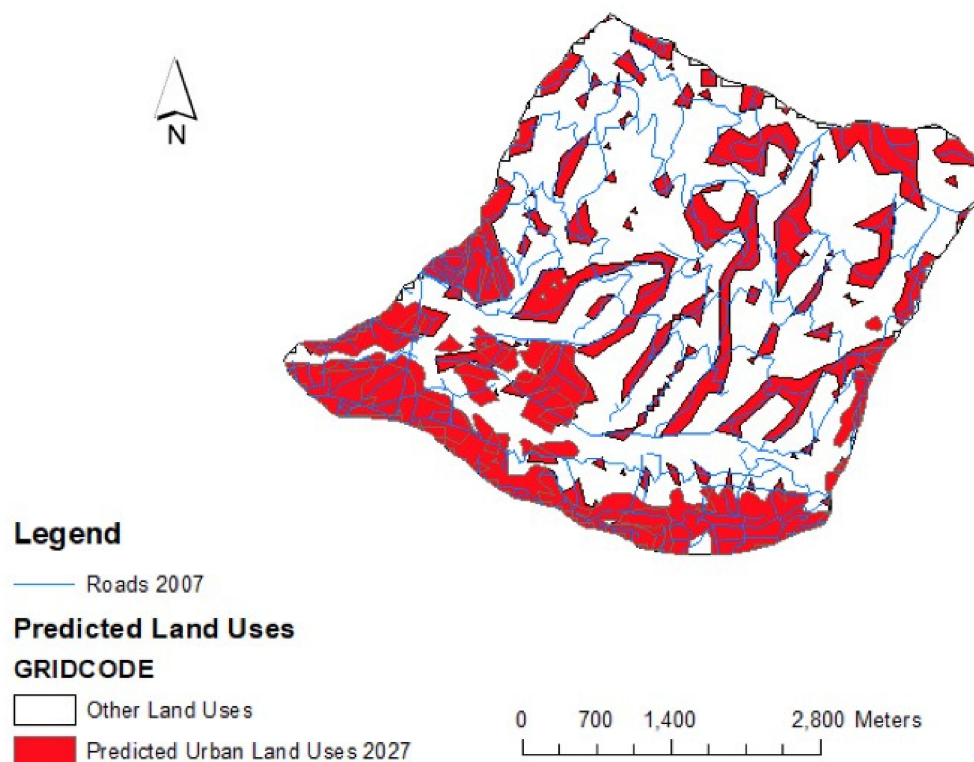


Figure 5. Predicted land use for the year 2027.

In Figure 5 the expansion of urban land uses is evident. Areas in red depict the predicted urban land use state for the year 2027. Additionally, on the map shown in Figure 5, we also present the road networks as they were in the year 2007. Land use change is performed for one type of change each time. This is mainly due to the way the ANNs work and perform their prediction. Each ANN calculates one output (urbanization in our case) for multiple inputs, which we regard as affecting the output. In order to study another type of land use change, we must train the ANN for the new type.

Finally, if we try to perform an overall land use change regardless of the type, we will have to add the errors performed in the prediction of each type separately.

4.2. Hydrologic and Sediment Yield Modelling

The precipitation heights generated from the design rain event with an 81-year return period and rain durations equal to 6, 12 and 24 h, were found to be equal to 66.6, 77.1 and 89.2 mm respectively; the ones produced from the 140-year return period storm event under the latter durations were found to be equal to 74.0, 85.6 and 99.0 mm. Moreover, all the storm event hyetographs were developed using the ABM method.

The soil maps that were acquired from the European Soil Data Centre were reclassified according to the four USDA Hydrologic soil groups based on soil texture [75]. The latter classification revealed that the *B*, *C* and *D* hydrologic soil groups encompass 77.2%, 20.1% and 2.7% of the study area respectively. The hydrologic soil group map was overlaid with the 1979 and 2007 reference land use maps and the 2027 LTM future urban sprawl forecast map in the GIS environment, so as to assign an individual *CN* number for AMC-II conditions to each possible combination of land use type and hydrologic soil group from published tables [69]. These individual curve number values for all the different hydrologic soil types and land use combinations within the catchment were used so as to generate a catchment area-weighted *CN* value equal to 65, 69 and 74 for the 1979, 2007 and 2027 land use maps respectively. The latter values were used to calculate the maximum potential for soil retention and the effective precipitation amount according to the SCS-CN method [69]; Figure 6 illustrates the effective precipitation of a 140-year 12-h design rain event for the year 1979 whereas Table 1 presents the amount of effective precipitation for all storm events and time periods.

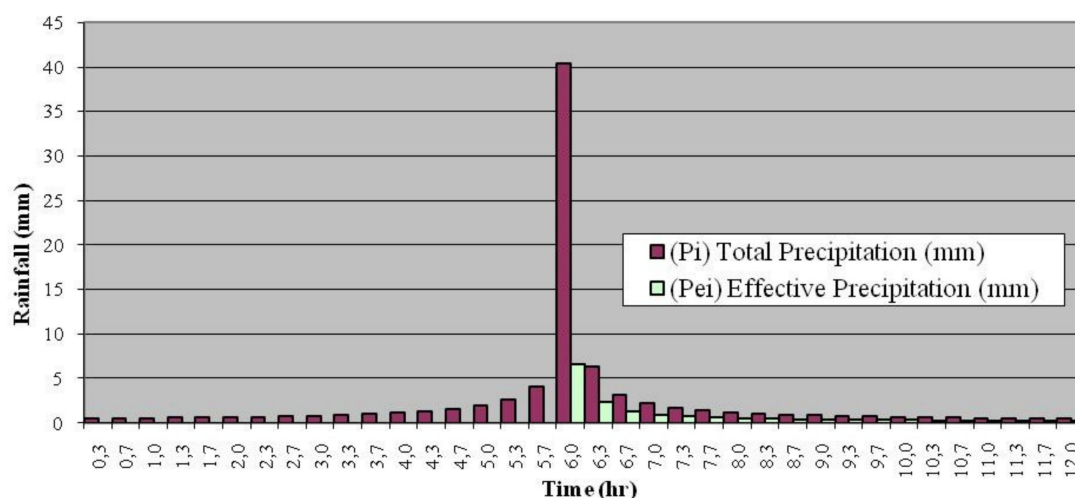


Figure 6. The effective precipitation hyetograph for a 140-year, 12-h duration storm event for the year 1979.

The SCS dimensionless unit hydrograph [30,63] for a 0.333 h rainfall duration storm event, which is equal to the ABM method incremental precipitation time step, was reduced for the years 1979, 2007 and 2027 and is illustrated in Figure 7. The differences in the shape of the unit hydrographs for the three time periods are solely due to urban expansion, recorded or forecasted, since all other drivers were set constant, as in 1979. As the urban sprawl expands over the decades, it is evident that the unit hydrograph's time of peak, lag time and duration decreases, whilst the peak discharge and flood volume increase.

By tying together the effective rainfall temporal distribution amounts, derived from the utilization of the ABM method, with the unit hydrograph, which corresponds to each time period (Figure 7), the discrete convolution method was applied and the flood hydrographs for all storm events and different historic and forecasted land use conditions were produced. The information regarding the

peak discharge, the time of peak and the discharge volume for each storm event is summarized in Table 1.

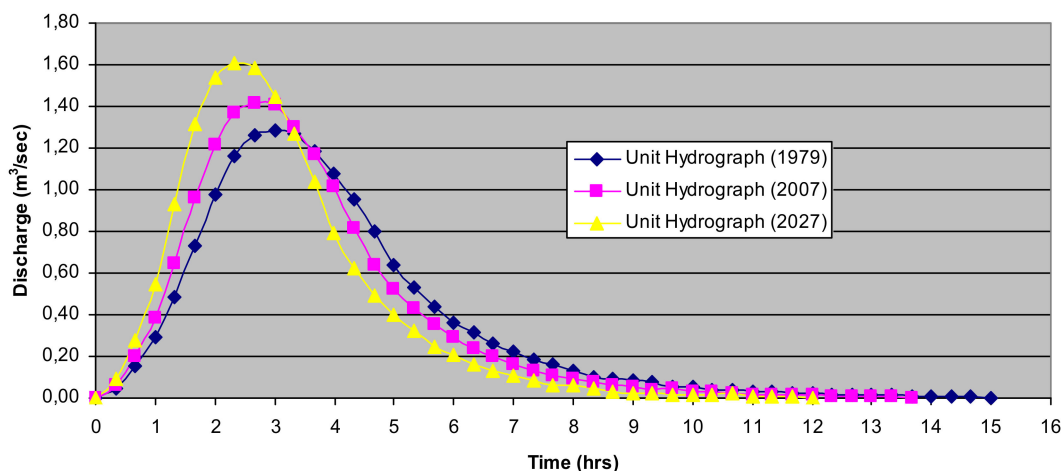


Figure 7. The unit hydrograph response to urban expansion.

Table 1 shows that the effective rainfall magnitude increase follows the urban sprawl increase, which is in line with the rainfall duration and return period increase. Compared to the pristine conditions of 1978, the peak discharge of the urban sprawl escalated at a range of 1.4 and 1.5 times for the year 2007 and could range from 2.2 to 2.6 times for the year 2027. However, it should be noted that, in the latter cases, as the rainfall duration increased, the peak flow was less affected, compared to the storm events of a short duration. Moreover, as the urban land expanded over the decades, the time of peak reduced in all cases, while the time of peak delayed as the rainfall duration increased. Furthermore, flood volume in response to urban expansion surged between 1.2 and 1.4 times for the year 2007 and could range from 1.6 to 2.1 times for the year 2027, compared to the 1979 reference period.

The peak discharge values and the discharge volumes from the 18 generated flood hydrographs were used to calculate the MUSLE model runoff factor. The *K* factor measures the soil susceptibility to both detachment and transportation caused by raindrops and runoff; it was obtained from the European Soil Data Centre 500-m resolution soil erodibility raster map [76], whilst its area weighted value for the study area was found equal to 0.024. The *K* factor was assumed to be constant over time since there were not possible to find any additional information's regarding its value for the 1978 conditions or the forecasted 2027 period. The topographic factor considers the effect of topography on erosion and relies on slope percentage and slope length, whilst the Moore and Burch (1986a,b) formula was used in ArcGIS to calculate the *LS* factor using the catchment's flow accumulation and slope in degrees 10-m grids [77,78]; it was found that the area-weighted *LS* was equal to 1.12.

The crop management factor depends on vegetation cover, which dissipates the raindrops' kinetic energy before impacting on soil surface; it was computed by allocating the appropriate *C* values, as recommended by [79], to the land use classes of the land use maps for the three time periods. In response to urban land expansion from 6% to 19% and 31% for the year 1979, 2007 and 2027 respectively the area weighted *C* values were evolved to 0.17, 0.27 and 0.39 respectively. The supporting practice indicates the rate of soil loss related to various practices, such as contouring, strip cropping, log terraces and so forth and was obtained from the European Soil Data Centre 100-m resolution conservation practice factor raster map [80], whilst its area weighted value for the study area was found equal to 0.98. Finally, the MUSLE/GIS coupling was used to compute the sediment yield for each of the simulated flood events, by multiplying the MUSLE input variables of Equation (7); Table 1 shows the computed soil loss volume per hectare for each simulation run.

The sediment yield modelling in this study indicated that, as the urbanization, return period and rainfall duration increased, the sediment volume increased too and compared to the 1979 pristine conditions, ranged from 0.19 to 0.48 t/ha for the year 2007 and from 0.47 to 1.05 t/ha for the 2027

future period. Moreover, the short duration storm events proportionally produced more sediment than the long duration precipitation events under the same land use conditions. Thus, the sediment production caused by short duration storm events is more sensitive compared to storm events of a longer duration.

Table 1. Summary of hydrologic and sediment yield modelling results.

Rainfall Duration	Return Period (T)	Year	CN	P_e	Peak Discharge (m ³ /s)	Time of Peak (h)	Discharge Volume (m ³)	Sediment Volume (t/ha)
6 h	Q ₅₀	1979	65	8.4	9.1	3.6	156,381	0.08
	Q ₅₀	2007	69	11.7	13.8	3.3	217,352	0.19
	Q ₅₀	2027	75	17.8	23.4	2.6	330,332	0.47
	Q ₁₀₀	1979	65	11.8	12.9	3.6	220,394	0.12
	Q ₁₀₀	2007	69	15.8	18.7	3.3	293,242	0.27
	Q ₁₀₀	2027	75	22.9	30.5	2.6	424,816	0.63
12 h	Q ₅₀	1979	65	13.2	12.0	6.7	245,740	0.12
	Q ₅₀	2007	69	17.5	17.6	6.3	323,359	0.27
	Q ₅₀	2027	75	25.0	29.1	5.6	461,781	0.64
	Q ₁₀₀	1979	65	17.4	16.1	6.7	322,184	0.16
	Q ₁₀₀	2007	69	22.3	22.8	6.3	411,723	0.36
	Q ₁₀₀	2027	75	30.7	36.4	5.6	568,037	0.81
24 h	Q ₅₀	1979	65	19.2	15.2	12.6	350,131	0.17
	Q ₅₀	2007	69	24.4	21.8	12.0	450,060	0.37
	Q ₅₀	2027	75	33.2	35.0	11.6	614,843	0.83
	Q ₁₀₀	1979	65	24.6	19.9	12.3	454,314	0.22
	Q ₁₀₀	2007	69	30.5	27.9	12.0	562,457	0.48
	Q ₁₀₀	2027	75	40.4	43.3	11.6	747,490	1.05

5. Discussion

The Land Transformation Model results indicate that by 2027 the urban land will encompass 31% of the catchment, whereas in 1979 and in 2007 the relevant percentages were 6% and 19% of the study area respectively; all other land use classes were set equal to 1979. Similar assumptions that each predictor variable pattern will remain constant over time, as in the initial land use map, are common in similar studies [81,82]. The model's low prediction accuracy (Kappa coefficient 0.15) in forecasting the urban expansion could be attributed to the small number of input variables that were incorporated in the model. Prediction patterns below 0.17 were also reported by [83], when they predicted olive grove cultivation patterns with the use of neural networks and GIS and attributed the low prediction ability to the small number of input variables. Moreover, Pijanowski et al. (2002) reported that even when 10 predictor variables were used on 100-m pixel resolution in the Land Transformation Model to assess future urban expansion, the model's prediction ability was 46% [81]. Furthermore, by comparing 13 applications of 9 different popular peer-reviewed land change models, Pontius et al. (2018) proved that, for 6 of the 13 models, the ratio of the intersection of the observed change and predicted change to the union of the observed change and predicted change was less than 0.15 [29].

Hydrologic modelling provides crucial information regarding the flood hydrograph characteristics which are used to correctly design hydraulic structures in small and ungauged catchments worldwide. Statistical analyses of hourly rainfall data by means of Gumbel's distribution provide the rainfall depth for different return periods [84], while the latter depth is rearranged over a time span through different techniques in order to develop design precipitation hyetographs [85]. The ABM hyetographs used in this study gain better results compared to other hyetograph computation methods because they are engineered from local rainfall datasets and not from rainfall distributions that are developed for other areas of the world and which in most cases have not been tested in the study area [86].

The CN values, compared to the ones reported by [12], are in close proximity with the 1979 pristine conditions and are underestimated for the 2007 period. This divergence for the 2027 time period is attributed to the fact that this study assumes that all land use types, including urban areas,

were constant as in 1979. For small catchments, the SCS-CN method [69] is the main approach used for estimating the infiltration capacity and runoff for various combinations of soil and land/use cover type [70]. The study highlighted that, as the urban development expanded over the decades, flood hydrograph peak flows and flood volume substantially increased by 1.4–2.6 times compared to the pre-urban conditions; the latter peak flow increase has also been documented in similar studies [6,40]. Additionally, it became evident that the longer the duration of the storm event the less effect there was on the peak flow. This observation is in agreement with the findings of [41], who reported that small floods and flood volumes would be more sensitive to urbanization.

The peak flow and runoff volume in the MUSLE model can be obtained through direct measurements from a water level stage recorder at the outlet of the catchments. However, in the poorly gauged mountainous areas of the Mediterranean region, these types of data are not usually available and are often extrapolated from hydrologic models [87], as in the case of the present study. For each individual storm event and urban sprawl conditions the MUSLE model was applied, in order to obtain the sediment volume, which ranged from 0.19 to 1.05 t/ha. The latter storm loss values are in line with reported individual storm soil loss values in different areas of the world [79].

6. Conclusions

Recent studies worldwide on urbanization prospects reveal that there is an upward shift on urban population rates, which is associated with urban land expansion [1–3]. In order to successfully manage urban growth and achieve sustainable development, proper catchment management, water resource planning and flood management must take into account the urban land expansion potential [41], otherwise the relevant structures may fail. In the present study, future urban land growth patterns for the catchment under study were revealed. The SCS-CN method indicated the hydrologic response of the catchment to urbanization in terms of peak discharge and flood volume escalation, while time of peak, lag time and duration decreased. Moreover, the MUSLE model revealed a significant sediment yield increase compared to the pristine conditions. As the urbanization of the world continues, such types of analysis are extremely important in order to design sustainable water constructions and minimize and mitigate the uncertainty and risks related to the urban sprawl. Future projects could focus on water structure failures associated to urban expansion.

Author Contributions: In this research, K.I. implemented the ANN in order to forecast the future urban expansion and D.M. performed the hydrologic and sediment yield modelling, while both authors equally contributed to the study design and the discussion of the results.

Funding: This research was funded by Aristotle University of Thessaloniki research committee under the program “Supporting Young Lecturers’ Research”.

Acknowledgments: D. Myronidis dedicates this work to the memory of his father, who passed away recently and laid the right foundations in order for his son to live a better life. The authors would like to thank the four anonymous referees and the editor for their detailed comments and suggestions which have greatly improved the quality of the paper. The authors would like to thank Amin Tayyebi for his support during the implementation of the Land Transformation Model.

Conflicts of Interest: The authors declare no conflict of interest.

References

1. United Nations. Department of Economic and Social Affairs, Population Division. World Urbanization Prospects: The 2018 Revision. Available online: <https://population.un.org/wup/Publications> (accessed on 30 September 2018).
2. Eurostat. Urban Europe Statistics on Cities, Towns and Suburbs. Available online: https://ec.europa.eu/eurostat/statistics-explained/index.php/Urban_Europe_%E2%80%94_statistics_on_cities,_towns_and_suburbs (accessed on 30 September 2018).
3. EPA. Urbanization and Population Change. Available online: <https://cfpub.epa.gov/roe/indicator.cfm?i=52> (accessed on 30 September 2018).

4. Huang, S.; Taniguchi, M.; Yamano, M.; Wang, C.-H. Detecting urbanization effects on surface and subsurface thermal environment—A case study of Osaka. *Sci. Total Environ.* **2009**, *407*, 3142–3152. [\[CrossRef\]](#)
5. Pauchard, A.; Aguayo, M.; Peña, E.; Urrutia, R. Multiple effects of urbanization on the biodiversity of developing countries: The case of a fast-growing metropolitan area (Concepción, Chile). *Biol. Conserv.* **2006**, *127*, 272–281. [\[CrossRef\]](#)
6. O'Driscoll, M.; Clinton, S.; Jefferson, A.; Manda, A.; McMillan, S. Urbanization Effects on Catchment Hydrology and In-Stream Processes in the Southern United States. *Water* **2010**, *2*, 605–648. [\[CrossRef\]](#)
7. Radice, A.; Longoni, L.; Papini, M.; Brambilla, D.; Ivov Ivanov, V. Generation of a Design Flood-Event Scenario for a Mountain River with Intense Sediment Transport. *Water* **2016**, *8*, 597. [\[CrossRef\]](#)
8. Radice, A.; Rosatti, G.; Ballio, F.; Franzetti, S.; Mauri, M.; Spagnolatti, M.; Garegnani, G. Management of flood hazard via hydro-morphological river modelling. The case of the Mallero in Italian Alps. *J. Flood Risk Manag.* **2013**, *6*, 197–209. [\[CrossRef\]](#)
9. Directive 2007/60/EC of the European Parliament and of the Council of 23 October 2007 on the Assessment and Management of Flood Risks. Available online: http://ec.europa.eu/environment/water/flood_risk/ (accessed on 30 September 2018).
10. Longoni, L.; Ivanov, V.I.; Brambilla, D.; Radice, A.; Papini, M. Analysis of the temporal and spatial scales of soil erosion and transport in a mountain basin. *IJEGE* **2016**, *2*, 17–30. [\[CrossRef\]](#)
11. Dow, C.L.; DeWalle, D.R. Trends in evaporation and Bowen ratio on urbanizing catchments in eastern United States. *Water Resour. Res.* **2000**, *36*, 1835–1843. [\[CrossRef\]](#)
12. Stathis, D.; Sapountzis, M.; Myronidis, D. Assessment of land use change effect on a design storm hydrograph using the SCS curve number method. *Fresenius Environ. Bull.* **2010**, *19*, 1928–1934. Available online: https://www.prt-parlar.de/download_feb_2010 (accessed on 30 September 2018).
13. Arnold, J.G.; Birkett, M.D.; Williams, J.R.; Smith, W.F.; McGil, H.N. Modelling the effects of urbanization on basin water yield and reservoir sedimentation. *Water Resour. Bull.* **1987**, *23*, 1101–1107. [\[CrossRef\]](#)
14. Pinaras, V.; Petalas, C.; Gikas, G.D.; Gemitzi, A.; Tsihrintzis, V.A. Hydrological and water quality modelling in a medium-sized basin using the Soil and Water Assessment Tool. *Desalination* **2010**, *250*, 274–286. [\[CrossRef\]](#)
15. National Research Council. *Advancing Land Change Modelling: Opportunities and Research Requirements*; The National Academies Press: Washington, DC, USA, 2014; pp. 1–152. [\[CrossRef\]](#)
16. Pontius, R.G.; Boersma, W.; Castella, J.-H.; Clarke, K.; De Nijs, T.; Dietzel, C.; Duan, Z.; Fotsing, E.; Goldstein, N.; Kok, K.; et al. Comparing the input, output and validation maps for several models of land change. *Ann. Reg. Sci.* **2008**, *42*, 11–37. [\[CrossRef\]](#)
17. Searchinger, T.; Heimlich, R.; Houghton, R.A.; Dong, F.X.; Elobeid, A.; Fabiosa, J.; Tokgoz, S.; Hayes, D.; Yu, T.H. Use of US croplands for biofuels increases greenhouse gases through emissions from land use change. *Science* **2008**, *319*, 1238–1240. [\[CrossRef\]](#) [\[PubMed\]](#)
18. Weiss, F.; Leip, A. Greenhouse gas emissions from the EU livestock sector: A life cycle assessment carried out with the CAPRI model. *Agric. Ecosyst. Environ.* **2012**, *149*, 124–134. [\[CrossRef\]](#)
19. Stevenson, J.R.; Villoria, N.; Byerlee, D.; Kelley, T.; Maredia, M. Green revolution research saved an estimated 18 to 27 million hectares from being brought into agricultural production. *Proc. Natl. Acad. Sci. USA* **2013**, *110*, 8363–8368. [\[CrossRef\]](#)
20. Cherubini, F. GHG balances of bioenergy systems—Overview of key steps in the production chain and methodological concerns. *Renew. Energy* **2010**, *35*, 1565–1573. [\[CrossRef\]](#)
21. Schmidinger, K.; Stehfest, E. Including CO₂ implications of land occupation in LCAs—method and example for livestock products. *Int. J. Life Cycle Assess.* **2012**, *17*, 962–972. [\[CrossRef\]](#)
22. Schmidt, J.H. Life cycle assessment of five vegetable oils. *J. Clean. Prod.* **2015**, *87*, 130–138. [\[CrossRef\]](#)
23. Audsley, E.; Brander, M.; Chatterton, J.; Murphy-Bokern, D.; Webster, C.; Williams, A. How Low Can We Go? An Assessment of Greenhouse Gas Emissions from the UK Food System and the Scope Reduction by 2050. WWF-UK. 2009. Available online: <http://dspace.lib.cranfield.ac.uk/handle/1826/6503> (accessed on 30 September 2018).
24. Vellinga, T.V.; Blonk, H.; Marinussen, M.; van Zeist, W.J.; de Boer, I.J.M.; Starmans, D. Methodology Used in FeedPrint: A Tool Quantifying Greenhouse Gas Emissions of Feed Production and Utilization. Wageningen UR Livestock Research. Report 674. 2013. Available online: <http://edepot.wur.nl/254098> (accessed on 30 September 2018).

25. Persson, U.M.; Henders, S.; Cederberg, C. A method for calculating a land use change carbon footprint (LUC-CFP) for agricultural commodities e applications to Brazilian beef and soy, Indonesian palm oil. *Glob. Chang. Biol.* **2014**, *20*, 3482–3491. [CrossRef]
26. De Rosa, M.; Knudsen, M.T.; Hermansen, J.H. A comparison of Land Use Change models: Challenges and future developments. *J. Clean. Prod.* **2016**, *113*, 183–193. [CrossRef]
27. Pijanowski, B.C.; Gage, S.H.; Long, D.T. A Land Transformation Model: Integrating Policy, Socioeconomics and Environmental Drivers using a Geographic Information System. In *Landscape Ecology: A Top Down Approach*; Sanderson, J., Ed.; CRC Press: Boca Raton, FL, USA, 1999; 272p, ISBN 9781566703680.
28. Pijanowski, B.C.; Pithadia, S.; Shellito, B.A.; Alexandridis, K. Calibrating a neural network-based urban change model for two metropolitan areas of the Upper Midwest of the United States. *Int. J. Geogr. Inf. Sci.* **2005**, *19*, 197–215. [CrossRef]
29. Pontius, R.G.; Castella, J.C.; De Nijs, T.; Duan, Z.; Fotsing, E.; Goldstein, N.; Kok, K.; Koomen, E.; Lippitt, C.D.; McConnell, W.; et al. Lessons and Challenges in Land Change Modelling Derived from Synthesis of Cross-Case Comparisons. In *Trends in Spatial Analysis and Modelling: Geotechnologies and the Environment*; Behnisch, M., Meinel, G., Eds.; Springer: Cham, Switzerland, 2018; Volume 19, pp. 143–164. ISBN 978-3-319-52520-4.
30. SCS (Soil Conservation Service). *SCS National Engineering Handbook, Section 4: Hydrology*; Soil Conservation Service: Washington, DC, USA, 1972; pp. 1–44.
31. Vaššová, D. Comparison of Rainfall-Runoff Models for Design Discharge Assessment in a Small Ungauged Catchment. *Soil Water Res.* **2013**, *8*, 26–33. Available online: <https://www.agriculturejournals.cz/publicFiles/84405.pdf> (accessed on 30 September 2018). [CrossRef]
32. Taylan, E.D.; Damcayiri, D. The prediction of runoff data for Kinikli basin by using the precipitation data with WMS. *Fresenius Environ. Bull.* **2017**, *26*, 7255–7263. Available online: https://www.prt-parlar.de/download_feb_2017 (accessed on 30 September 2018).
33. Williams, J.R. Sediment-Yield Prediction with Universal Equation Using Runoff Energy Factor. In *Present and Prospective Technology for Predicting Sediment Yield and Sources*; US Department of Agriculture, Agriculture Research Service: Washington, DC, USA, 1975; pp. 244–252.
34. Sadeghi, S.H.R.; Mizuyama, T. Applicability of the Modified Universal Soil Loss Equation for prediction of sediment yield in Khanmirza catchment, Iran. *Hydrol. Sci. J.* **2007**, *52*, 1068–1075. [CrossRef]
35. Pandey, A.V.; Chowdary, V.M.; Mal, B.C. Sediment yield modelling of an agricultural catchment using MUSLE, remote sensing and GIS. *Paddy Water Environ.* **2009**, *7*, 105–113. [CrossRef]
36. Kaffas, K.; Hrisanthou, V. Computation of hourly sediment discharges and annual sediment yields by means of two soil erosion models in a mountainous basin. *Int. J. River Basin Manag.* **2017**. [CrossRef]
37. Radice, A.; Giorgetti, E.; Brambilla, D.; Longoni, L.; Papini, M. On Integrated Sediment Transport Modelling for Flash Events in Mountain Environments. *Acta Geophys.* **2012**, *60*, 191–213. [CrossRef]
38. Tang, Z.; Engel, B.A.; Lim, K.J.; Pijanowski, B.C.; Harbor, J. Minimizing the impact of urbanization on long term runoff. *J. Am. Water Resour. Assoc.* **2005**, *41*, 1347–1359. [CrossRef]
39. Wayland, K.G.; Hyndman, D.W.; Boutt, D.; Pijanowski, B.C.; Long, D.T. Modelling the impact of historical land uses on surface-water quality using groundwater flow and solute-transport models. *Lakes Reserv. Res. Manag.* **2002**, *7*, 189–199. [CrossRef]
40. Lin, Y.-P.; Hong, N.-M.; Wu, P.-J.; Wu, C.-F.; Verburg, P.-H. Impacts of land use change scenarios on hydrology and land use patterns in the Wu-Tu catchment in Northern Taiwan. *Landsc. Urban Plan.* **2007**, *80*, 111–126. [CrossRef]
41. Du, J.; Qian, L.; Rui, H.; Zuo, T.; Zheng, D.; Xu, Y.; Xu, C.-Y. Assessing the effects of urbanization on annual runoff and flood events using an integrated hydrological modelling system for Qinhuai River basin, China. *J. Hydrol.* **2012**, *464–465*, 127–139. [CrossRef]
42. Hellenic Statistical Authority. 2011 Population and Housing Census for the Resident, De Jure (Registered) and De Facto population of Greece. Available online: <http://www.statistics.gr/en/2011-census-pop-hous> (accessed on 30 September 2018).
43. Zhang, W.; Montgomery, D.R. Digital elevation model grid size, landscape representation and hydrologic simulations. *Water Resour. Res.* **1994**, *30*, 1019–1028. [CrossRef]
44. Strahler, A.N. *Quantitative Geomorphology of Drainage Basins and Channel Networks, Handbook of Applied Hydrology*; McGraw-Hill: New York, NY, USA, 1964; pp. 439–476.

45. Sapountzis, M.; Koniaris, N.; Schizas, A.; Adamidou, M. Analysis of the extreme rainfall events in the catchments “Konstantinidi” and “Anotoumpas” at the urban forest of Thessaloniki. In Proceedings of the 10th International Hydrogeological Congress of Greece, Thessaloniki, Greece, 8–10 October 2014; pp. 267–276.
46. Koppen, W. *Grundriss der Klimakunde*; Walter de Gruyter: Berlin, Germany, 1931; pp. 1–44.
47. Stathis, D.; Mavromatis, T. Characteristics of Precipitation in Thessaloniki Area, North Greece. *Fresenius Environ. Bull.* **2009**, *18*, 1–6. Available online: https://www.prt-parlar.de/download_feb_2009 (accessed on 30 September 2018).
48. Ballabio, C.; Panagos, P.; Montanarella, L. Mapping topsoil physical properties at European scale using the LUCAS database. *Geoderma* **2016**, *261*, 110–123. [[CrossRef](#)]
49. Myronidis, D.; Stathis, D.; Sapountzis, M. Post-Evaluation of Flood Hazards Induced by Former Artificial Interventions along a Coastal Mediterranean Settlement. *J. Hydrol. Eng.* **2016**, *21*. [[CrossRef](#)]
50. Koutroumanidis, T.; Ioannou, K.; Arabatzis, G. Predicting fuelwood prices in Greece with the use of ARIMA models, artificial neural networks and a hybrid ARIMA-ANN model. *Energy Policy* **2009**, *37*, 3627–3634. [[CrossRef](#)]
51. Ioannou, K.; Arabatzis, G.; Lefakis, P. Predicting the prices of forest energy resources with the use of Artificial Neural networks (ANNs). The case of conifer fuel wood in Greece. *J. Environ. Prot. Ecol.* **2009**, *10*, 678–694.
52. Ioannou, K.; Biribilis, D.; Lefakis, P. A method for predicting the possibility of ring shake appearance on standing chestnut trees (*Castaneasativa* MILL.). *J. Environ. Prot. Ecol.* **2011**, *12*, 295–304.
53. Koutroumanidis, T.; Ioannou, K.; Zafeiriou, E. Forecasting bank stock market prices with a hybrid method: The case of Alpha bank. *J. Bus. Econ. Manag.* **2011**, *12*, 144–163. [[CrossRef](#)]
54. Tang, Z.; Engel, B.A.; Pijanowski, B.C.; Lim, K.J. Forecasting land use change and its environmental impact at a catchment scale. *J. Environ. Manag.* **2005**, *76*, 35–45. [[CrossRef](#)]
55. Skapura, D. *Building Neural Networks*, 1st ed.; ACM Press: New York, NY, USA, 1996; ISBN 13 978-0201539219.
56. Zell, A.; Mamier, G.; Vogt, M.; Mache, N.; Hübner, R.; Döring, S.; Herrmann, K.; Soye, T.; Schmalzl, M.; Sommer, T.; et al. Stuttgart neural network simulator. In *Neural Network Simulation Environments*; Skrzypek, J., Ed.; Springer: Boston, MA, USA, 1994; Volume 254, pp. 165–186. ISBN 978-1-4613-6180-0.
57. Argyrakis, P. *Neural Networks and Applications*; Hellenic Open University: Patras, Greece, 2001. (In Greek)
58. Brown, D.; Pijanowski, B.; Duh, J. Modelling the Relationships between Land Use and Land Cover on Private Lands in the Upper Midwest. *J. Environ. Manag.* **2001**, *59*, 247–263. [[CrossRef](#)]
59. Pijanowski, B.C.; Alexandridis, K.T.; Mueller, D. Modeling urbanization in two diverse regions of the world. *J. Land Use Sci.* **2006**, *1*, 83–108. [[CrossRef](#)]
60. Myronidis, D.; Fotakis, D.; Sgouropoulou, K.; Sapountzis, M.; Stathis, D. Checking a culvert suitability for flood wave routing within the framework of the EU flood directive. In Proceedings of the 7th International Conference on Information and Communication Technologies in Agriculture, Food and Environment, Kavala, Greece, 17–20 September 2015; pp. 146–153.
61. Methods, H.; Dyhouse, G.; Hatchett, J.; Benn, J. *Floodplain Modeling Using HEC-RAS*; Haestad Methods, Inc: Waterbury, CT, USA, 2003; ISBN 978-0971414105.
62. Myronidis, D.; Fotakis, D. Utilizing 3D solid modelling tools for simplified designing of a small concrete Gravity Dam. *Int. J. Sustain. Agric. Manag. Inform.* **2015**, *1*, 351–357. [[CrossRef](#)]
63. Chow, V.T.; Maidment, D.R.; Mays, L.W. *Applied Hydrology*; McGraw-Hill Book Company: New York, NY, USA, 1988; ISBN 0070108102.
64. Mishra, A.; Kar, S.; Singh, V.P. Prioritizing Structural Management by Quantifying the Effect of Land Use and Land Cover on Catchment Runoff and Sediment Yield. *Water Resour. Manag.* **2007**, *21*, 1899–1913. [[CrossRef](#)]
65. Mongil-Manso, J.; Navarro-Hevia, J.; Díaz-Gutiérrez, V.; Cruz-Alonso, V.; Ramos-Díez, I. Badlands forest restoration in Central Spain after 50 years under a Mediterranean-continental climate. *Ecol. Eng.* **2016**, *97*, 313–326. [[CrossRef](#)]
66. Xiang-zhou, X.; Hong-wu, Z.; Ouyang, Z. Development of check-dam systems in gullies on the Loess Plateau, China. *Environ. Sci. Policy* **2004**, *7*, 79–86. [[CrossRef](#)]
67. Gumbel, E.J. *Statistics of Extremes*; Columbia University Press: New York, NY, USA, 1958; ISBN 0486436047.
68. Sutcliffe, J.V. *Methods of Flood Estimation: A Guide to the Flood Studies Report*; IH Report No. 49; Institute of Hydrology: Wallingford, UK; 50p, Available online: <http://nora.nerc.ac.uk/id/eprint/5776> (accessed on 30 September 2018).

69. USDA/NRC. *Urban Hydrology for Small Catchments TR-55*; Technical Release 55; Washington, DC, USA. Available online: https://www.nrcs.usda.gov/Internet/FSE_DOCUMENTS/stelprdb1044171.pdf (accessed on 30 September 2018).
70. Al-Zahrani, M.; Al-Areeq, A.; Sharif, H.O. Estimating urban flooding potential near the outlet of an arid catchment in Saudi Arabia. *Geomat. Nat. Hazards Risk*. **2017**, *8*, 672–688. [CrossRef]
71. Ponce, V.M. *Engineering Hydrology: Principles and Practice*, 1st ed.; Prentice Hall: Englewood Cliffs, NJ, USA, 1989; 640p, ISBN 978-0132778312.
72. Moench, A.F.; Kisiel, C.C. Application of the convolution relation to estimating recharge from an ephemera stream. *Water Resour. Res.* **1970**, *6*, 1087–1094. [CrossRef]
73. Bruen, M.; Dooge, J.C.I. An efficient and robust method for estimating unit hydrograph ordinates. *J. Hydrol.* **1984**, *70*, 1–24. [CrossRef]
74. Wischmeier, W.H.; Smith, D.D. *Predicting Rainfall Erosion Losses—A Guide to Conservation Planning*; Agricultural Handbook No. 537; USDA; Forest Service: Washington, DC, USA. Available online: <https://data.globalchange.gov/report/usda-aghandbook-537> (accessed on 30 September 2018).
75. Rawls, W.J.; Brakensiek, D.L.; Saxton, K.E. Estimation of soil water properties. *Trans. ASAE* **1982**, *25*, 1316–1320. [CrossRef]
76. Panagos, P.; Meusburger, K.; Ballabio, C.; Borrelli, P.; Alewell, C. Soil erodibility in Europe: A high-resolution dataset based on LUCAS. *Sci. Total Environ.* **2014**, *479–480*, 189–200. [CrossRef]
77. Moore, I.; Burch, G. Physical basis of the length-slope factor in the Universal Soil Loss Equation. *Soil Sci. Soc. Am. J.* **1986**, *50*, 1294–1298. Available online: <https://dl.sciencesocieties.org/publications/sssaj/pdfs/50/5/SS0500051294> (accessed on 30 September 2018). [CrossRef]
78. Moore, I.; Burch, G. Modelling erosion and deposition: Topographic effects. *Trans. ASAE* **1986**, *29*, 1624–1630. [CrossRef]
79. Morgan, R. *Soil Erosion and Conservation*, 3rd ed.; Blackwell Publishing: Malden, MA, USA, 2005; 316p, ISBN 978-1405117814.
80. Panagos, P.; Van Liedekerke, M.; Jones, A.; Montanarella, L. European Soil Data Centre: Response to European policy support and public data requirements. *Land Use Policy* **2012**, *29*, 329–338. [CrossRef]
81. Pijanowski, B.C.; Brown, D.G.; Shellito, B.A.; Manikd, G.A. Using neural networks and GIS to forecast land use changes: A Land Transformation Model. *Comput. Environ. Urban Syst.* **2002**, *26*, 553–575. [CrossRef]
82. Tayyebi, A.; Delavar, M.R.; Saeedi, S.; Amini, J.; Alinia, H. Monitoring land use change by multi-temporal landsat remote sensing imagery. In Proceedings of the ISPRS Archives, Beijing, China, 3–11 July 2008; Volume XXXVII-B7, pp. 1037–1042. Available online: http://www.isprs.org/proceedings/XXXVII/congress/7_pdf/5_WG-VII-5/54.pdf (accessed on 30 September 2018).
83. Vafeidis, A.T.; Koukoulas, S.; Gatsis, I.; Gkoltsiou, K. Forecasting Land Use Changes with the Use of Neural Networks and GIS. In Proceedings of the IEEE International Geoscience and Remote Sensing Symposium, Barcelona, Spain, 23–28 July 2007. [CrossRef]
84. Zope, P.E.; Eldho, T.I.; Jothiprakash, V. Hydrological impacts of land use–land cover change and detention basins on urban flood hazard: A case study of Poisar River basin, Mumbai, India. *Nat. Hazards*. **2017**, *87*, 1267–1283. [CrossRef]
85. Grimaldi, S.; Petroselli, A.; Serinaldi, F. Design hydrograph estimation in small and ungauged catchments: Continuous simulation method versus event-based approach. *Hydrol. Process.* **2011**, *26*, 3124–3134. [CrossRef]
86. Koutsoyiannis, D.; Xanthopoulos, T. Engineering Hydrology. Available online: <http://hdl.handle.net/11419/5888> (accessed on 30 September 2018).
87. Cambazoglu, M.; Gogus, M. Sediment Yields of Basins in the Western Black Sea Region of Turkey. *Turk. J. Eng. Environ. Sci.* **2004**, *28*, 355–367. Available online: <http://journals.tubitak.gov.tr/engineering/issues/muh-04-28-6/muh-28-6-2-0403-8.pdf> (accessed on 30 September 2018).

